fire

MDPI

Article

Investigating Drought Events and Their Consequences in Wildfires: An Application in China

Song Yang [1,2,†], **Aicong Zeng** [1,2,†], **Mulualem Tigabu** [3], **Guangyu Wang** [4], **Zhen Zhang** [1,2], **He Zhu** [1,2] **and Futao Guo** [1,2,*]

1   College of Forestry, Fujian Agriculture and Forestry University, Fuzhou 350002, China; fjzac13655014632@126.com (A.Z.); zhuhe19990116@126.com (H.Z.)
2   3S Technology and Resource Optimization Utilization Key Laboratory of University, Fuzhou 350002, China
3   Southern Swedish Forest Research Centre, Swedish University of Agricultural Sciences, P.O. Box 190, SE-234 22 Lomma, Sweden
4   Department of Forest Resources Management, Faculty of Forestry, University of British Columbia, Vancouver, BC V6T 1Z4, Canada
*   Correspondence: guofutao@126.com
†   These authors contributed equally to this work.

Abstract: Understanding the impact of drought on fire dynamics is crucial for assessing the potential effects of climate change on wildfire activity in China. In this study, we present a series of multiple linear regression (MLR) models linking burned area (BA) during mainland China's fire season from 2001 to 2019, across seven regions, to concurrent drought, antecedent drought, and time trend. We estimated burned area using Collection 6 Moderate Resolution Imaging Spectradiometer (MODIS) and drought indicators using either the Standardized Precipitation Evapotranspiration Index (SPEI) or the self-calibrated Palmer Drought Severity Index (sc-PDSI). Our findings indicate that the wildfire season displays a spatial variation pattern that increases with latitude, with the Northeast China (NEC), North China (NC), and Central China (CC) regions identified as the primary areas of wildfire occurrence. Concurrent and antecedent drought conditions were found to have varying effects across regions, with concurrent drought as the dominant predictor for NEC and Southeast China (SEC) regions and antecedent drought as the key predictor for most regions. We also found that the Northwest China (NWC) and CC regions exhibit a gradual decrease in burned area over time, while the NEC region showed a slight increase. Our multiple linear regression models exhibited a notable level of predictive power, as evidenced by the average correlation coefficient of 0.63 between the leave-one-out cross-validation predictions and observed values. In particular, the NEC, NWC, and CC regions demonstrated strong correlations of 0.88, 0.80, and 0.76, respectively. This indicates the potential of our models to contribute to the prediction of future wildfire occurrences and the development of effective wildfire management and prevention strategies. Nevertheless, the intricate relationship among fire, climate change, human activities, and vegetation distribution may limit the generalizability of these findings to other conditions. Consequently, future research should consider a broad range of factors to develop more comprehensive models.

Keywords: drought; fire dynamics; climate change

1. Introduction

Wildfire plays a significant part in the terrestrial carbon cycle and ecosystem functioning as a natural disturbance process that is prevalent across the majority of the earth's surface [1,2]. The frequency and severity of wildfires have grown globally in recent decades as result of climate change [3,4], resulting in significant economic and human losses as well as substantial environmental pollution [5,6]. Understanding how wildfires respond to climate change is important for monitoring, predicting, and developing wildfire prevention and control programs.

Weather conditions mostly affect the likelihood of wildfires by controlling the drying of fuel and loading of fuel, provided that the ignition source is unrestricted [7,8]. Wildfires often occur in moderately humid areas. On the one hand, the drying level is sufficiently high in comparison to the local humid state, allowing for a shift in local fuel flammability. On the other hand, drought episodes occur frequently to occasionally and thus dry fuels, but they do not continue to dry so as to limit the production of fuel [9]. Despite the fact that vegetation can typically create enough fuel in consistently humid environments, wildfires typically do not occur frequently. However, in regions that are consistently dry, prolonged drought frequently prevents the accumulation of fuels [10–12].

Prior research indicates that concurrent climate conditions, including temperature [13,14], can have an effect on fire activity, while precipitation during the preceding 1–2 growing seasons has been found to influence biomass production and subsequent fire activity [10,15]. These studies support the notion that fires are influenced not only by concurrent climate conditions but also by antecedent climate variables. However, a comprehensive understanding of the year-to-year potential links between both concurrent and antecedent climate variables and fire activity in different regions of China remains incomplete.

In the context of China, recent studies have focused on examining the relationships between fire activities and climatic variables at different temporal scales (monthly, seasonal, and annual) using provinces as the spatial scale [16]. The findings of these studies suggest that models utilizing drought indices, such as the Palmer Drought Severity Index (PDSI) and Standardized Precipitation Index (SPI), demonstrate a higher degree of accuracy in predicting annual variations in fires compared to models relying on other climatic variables. However, it is important to note that this research has certain limitations, such as the failure to analyze the connection between fires and preceding drought conditions. Additionally, both the PDSI and SPI indices are subject to various known limitations. The PDSI, for instance, is built upon the concept of water balance, encompassing factors such as prior precipitation, moisture supply, runoff, and surface-level evaporation demand [17]. The calculation of the PDSI index involves a general formula that incorporates empirical constants. These constants were established by Palmer [18] based on a limited number of locations, leading to inconsistent behavior of the PDSI index in other regions and posing challenges for the development of drought-fire models. In contrast, the self-calibrated Palmer Drought Severity Index (sc-PDSI) dynamically calculates these empirical constants, automatically adjusting the behavior of the index across different regions. On the other hand, the SPI index is solely based on precipitation data. It relies on two key assumptions: (1) precipitation variability is significantly greater than that of other variables (e.g., temperature and PET), and (2) the other variables exhibit stationarity, meaning they have no temporal trend [19]. However, it is worth noting that the climate in China has not only experienced a higher rate of warming in recent decades compared to the global trend [20,21], but it is also projected to worsen under future emission scenarios [22]. To address the combined effects of precipitation and temperature variability in drought assessment, the Standardized Precipitation Evapotranspiration Index (SPEI) is utilized. The SPEI incorporates precipitation and temperature data, offering the advantage of combining a multiscale character with the capacity to account for temperature variability's impact on drought evaluation [17].

Quantifying spatiotemporal variations in the effects of concurrent and antecedent drought conditions on fires is crucial for gaining further insights into fire management strategies. Specifically, identifying the duration and timing of droughts that have the most significant impact on fires as well as the influence of antecedent drought conditions is an area that remains understudied in China. Such information would significantly benefit policymakers and civil protection agencies in improving early warning systems and implementing more effective fire management strategies. This study aims to investigate the suitability of a simple drought-fire model for modeling annual changes in burned area (BA) in China and to identify the drought index time window that exerts a more significant influence on BA.

2. Data and Methods

2.1. Study Area

The Chinese mainland is geographically divided into seven distinct regions: Northeast China (NEC), Northwest China (NWC), North China (NC), Southwest China (SWC), Central China (CC), South China (SC), and Southeast China (SEC) [23,24]. These regions were chosen as the spatial units of analysis for several reasons. Adopting a region-based division approach offers the potential to effectively disseminate the findings of this study to national-level policymakers and personnel involved in forest-fire management. In terms of elevation, NEC, CC, and SEC generally have elevations below 500 m (Figure 1a). SWC, western SC, and northern NWC comprise mountainous and plateau areas, with elevations reaching up to 3000 m (excluding the lower Sichuan Basin in northeast SC). The major vegetation types in the study area include needle and broadleaf forests in NEC, SEC, SC, and southern CC, while northern NC is predominantly covered by grasslands.
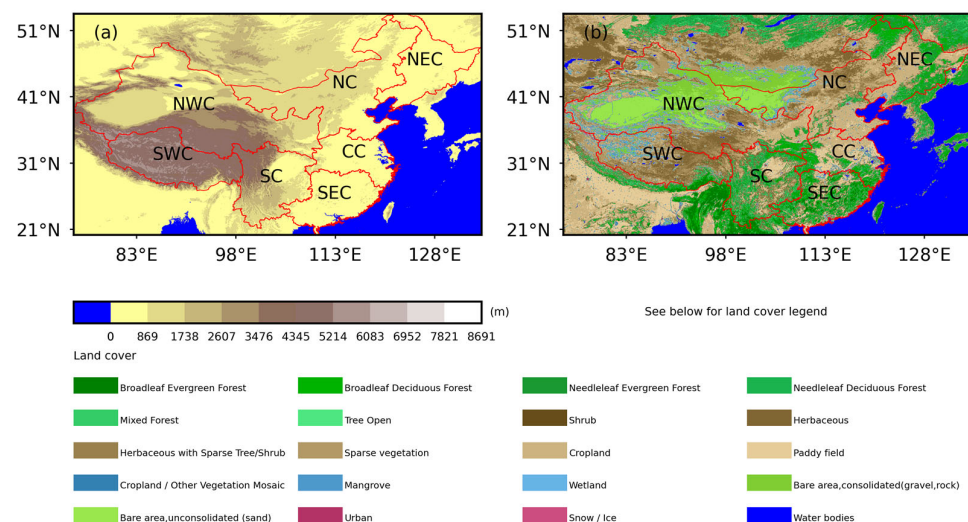

Figure 1. Defined Regions in China with Elevation (**a**) and Land Cover (**b**). The elevation and land-cover data utilized to generate this figure were obtained from the International Steering Committee for Global Mapping (ISCGM) and can be accessed at https://globalmaps.github.io/ (accessed on 28 October 2022).

The precipitation distribution in China follows a general pattern of decreasing from southeast to northwest, with the highest concentration of precipitation occurring between April and October. The regions of North China (NC) and Northwest China (NWC) receive the least amount of precipitation, with the highest monthly precipitation being less than 100 mm. Conversely, Southeast China (SEC), Southwest China (SWC), and Central China (CC) experience abundant precipitation, primarily influenced by the subtropical monsoon climate (Figure 2). In terms of temperature distribution, China exhibits high temperatures during summer and notable variations between the northern and southern regions in winter. During January–March and November–December, the temperature in Northeast China (NEC), Northwest China (NWC), North China (NC), and Southwest China (SWC) remains below 0 °C. On the other hand, South China (SC), Central China (CC), and Southeast China (SEC) maintain temperatures above 0 °C throughout the year (Figure 2).

2.2. Data

Burned area (BA) data were derived from the collection 6 Moderate Resolution Imaging Spectroradiometer (MODIS) Burned Area (MCD64MCQ). The data are composed of monthly BA from 2001 to 2019 since the numerical values were lacking in the summer of 2020 due to a satellite sensor issue. The MCD64MCQ data product is convenient for regional modelling under continuous roughly spatiotemporal scale with spatial resolution of

0.25. The accuracy of the data was validated by numerous independent investigations using the high-resolution Advanced Spaceborne Thermal Emission and Reflection Radiometer (ASTER) image. Detailed information about this issue can be found elsewhere [25–28].
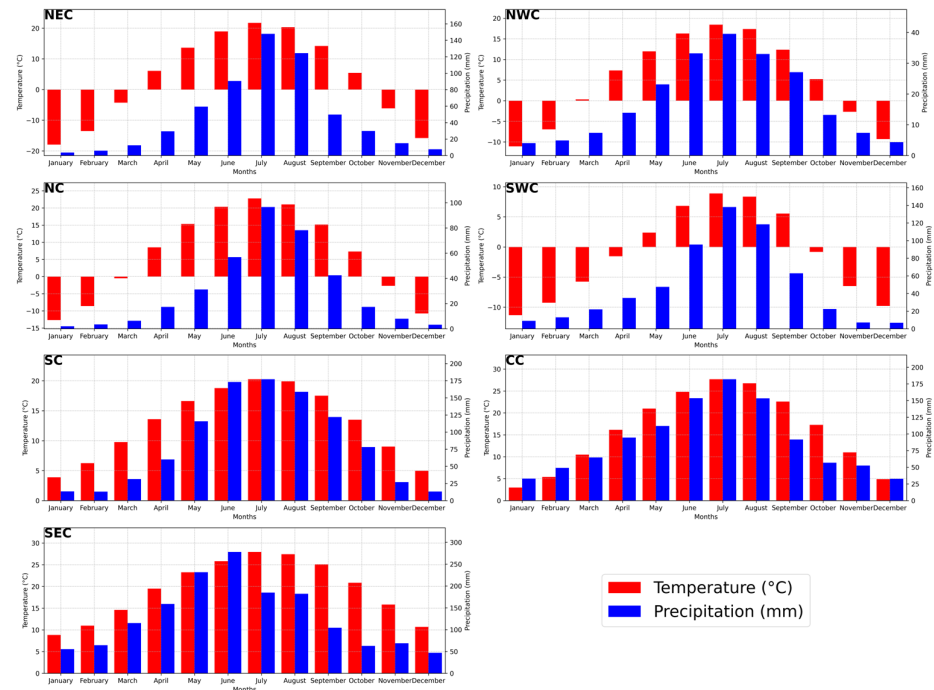
Figure 2. This figure depicts the monthly temperature and precipitation patterns in China.

Elevation, land cover, temperature, and precipitation data play a crucial role in providing the hydrological and topographical context for the study area. The elevation and land-cover data were sourced from the International Steering Committee for Global Mapping (ISCGM) through their website at https://globalmaps.github.io/ (accessed on 28 October 2022). Temperature and precipitation data were derived from the gridded Climatic Research Unit (CRU) Time-series (TS) dataset version 4.05 [29], which is also used for calculating the SPEI and sc-PDSI datasets by the University of East Anglia Climatic Research Unit. For assessing drought conditions, we utilized the Standardized Precipitation Evapotranspiration Index (SPEI) [19] and the self-calibrated Palmer Drought Severity Index (sc-PDSI) [17]. The sc-PDSI, similar to the PDSI, incorporates autoregression, where the sc-PDSI value for a specific month is determined by the weighted sum of the previous month's sc-PDSI and the moisture anomaly index. The moisture anomaly index is computed using the moisture departure (the difference between actual precipitation and climatically appropriate precipitation) and climatic characteristics. Palmer [18] derived empirical constants for climatic characteristics and duration factors based on data from several U.S. stations, while Wells [17] introduced a method to automatically adjust these empirical constants for a specific location using historical climate data.

The SPEI, on the other hand, combines precipitation and temperature data, offering the advantage of capturing temperature variability's influence on drought assessment across multiple time scales [17]. The calculation procedure involves a climatic water balance, accumulation of deficit/surplus at different time scales, and adjustment to a log-logistic probability distribution [17]. We obtained the SPEI (version 2.7) and sc-PDSI datasets from the University of East Anglia Climatic Research Unit (UEACRU), with a spatial resolution of 0.5 degrees [30,31]. Overall, the combination of these datasets enables a comprehensive analysis of the hydrological and climatic conditions, which is essential for understanding drought dynamics in the study area.

2.3. Methodology

Many previous studies have attempted to investigate the effects of climate on wildfires at the original spatial scales of the dataset [32–34]. However, the process by which climate affects wildfire is very complex, and the smaller spatial scale is very sensitive to human factors, vegetation factors, and other arbitrary factors related to ignition. Therefore, the Chinese mainland is divided into seven distinct regions.

Wildfire occurrence has obvious seasonal and continuous characteristics that vary with geographical location due to human and climatic factors [35,36]. We defined the fire season as the shortest continuous calendar month during which each region has more than 80% BA over 2001–2019 [37,38]. The fire seasons of the NEC, NWC, NC, SWC, CC, SC, and SEC, respectively, span from February to October (2–10), February to July (2–7), March to September (3–9), January to April (1–4), May to June (5–6), February to April (2–4), and January to November (1–11).

We used the SPEI and sc-PDSI indices, respectively, as drought indicators, and we processed the data as follows: We normalized the positively biased BA variables by applying a log transformation. The drought indicator is quantified by computing the mean of the indices over a duration of several months and expressed as $\text{Drought}_{c,m,b}$. Here, m denotes the month used for drought indicator computation ($\text{fireseason}_{start}$ and fireseason_{end}), c represents the number of months, and b signifies the buffer period prior to the onset of the fire season. For concurrent drought, c is multiple months in the fire season ($\text{fireseason}_{length}$), m is the month when the fire season ends, and b is 0. For antecedent drought, c ranges from 1 to 12 months, m is the month when the fire season starts, and b ranges from 2 to 14 months. For example, $\text{Drought}_{3,6,2}$ represents the average value from January to March.

Multiple linear regression (MLR) is commonly employed for establishing interannual climate-fire models owing to its ease of interpretation and the avoidance of overfitting associated with the use of non-linear models. For each region in China, we used the following drought-BA model to express the potential relationship between the annual variation of fire season BA and drought indices (SPEI, sc-PDSI), where the number of predictors is limited to a maximum of three (concurrent drought indicator, antecedent drought indicator, and time term):

$$\log[\text{BA}(i,t)] = \beta_0(i) + \beta_1(i) \cdot \text{Drought}_{c,m,0}(i,t) + \beta_2(i) \cdot \text{Drought}_{c,m,b}(i,t) + \beta_3(i) \cdot \text{T}(t) + \varepsilon(i,t) \tag{1}$$

where $\text{BA}(i,t)$ is the predicted BA in the i region and year t. β_0 is the intercept; β_1 represents the sensitivity of BA in each region to concurrent dry conditions as summarized by the drought index; β_2 represents the sensitivity of BA in each region to antecedent dry conditions as summarized by the drought index; β_3 is the coefficient of the time term T (in years) that characterizes the temporal trends of BA, thus taking into account the possible influence of slowly changing factors over the study period; ε is a stochastic noise term that captures all other factors that influence BA except for drought index.

For each region, we considered these combinations of predictors: concurrent drought only, antecedent drought only, concurrent drought plus time, antecedent drought plus time, and concurrent and antecedent drought plus time. We employed the Akaike information criterion (AIC) [39] to select the models with the lowest AIC values. The AIC allows us to assess the quality of each model relative to the others in a given collection of models. The calculation method for the AIC value of each multiple linear regression (MLR) model is as follows:

$$\text{AIC} = 2k - 2\ln(\hat{L})$$

Here, *L* represents the maximum value of the likelihood function for the model, and *k* represents the number of parameters to be estimated in the model. The AIC combines the goodness of fit, as measured by the likelihood function, with a penalty that increases as the number of estimated parameters increases. This ensures that the AIC considers both model

fit and complexity. To further evaluate the selected model, we performed leave-one-out cross-validation. This validation technique involves systematically leaving out one data point at a time, fitting the model to the remaining data, and then assessing the model's predictive performance using the left-out data point. This process is repeated for each data point, and the overall performance is evaluated. For a step-by-step description of the model development, selection, and evaluation process, please refer to Figure 3, which provides a visual representation of the procedure.
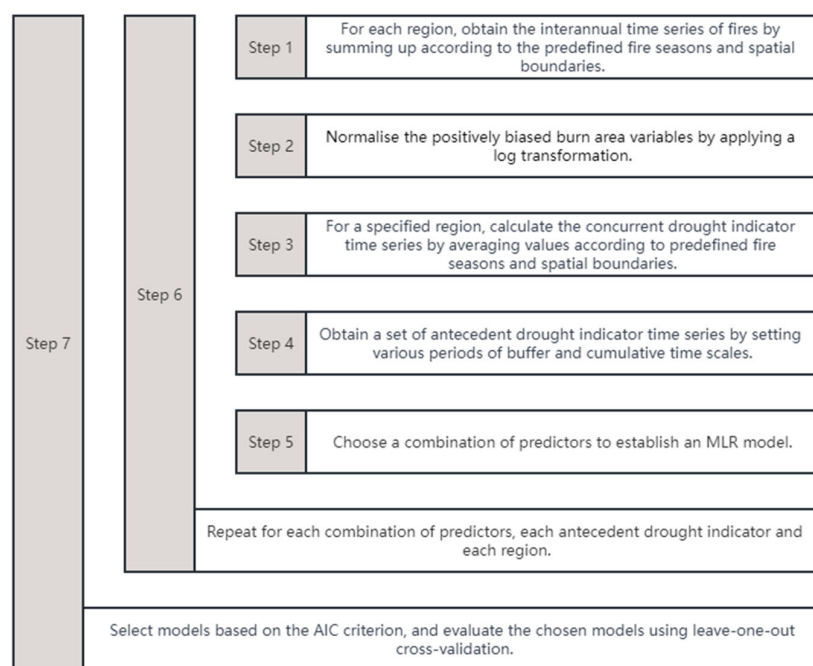
**Figure 3.** Step-by-step description of model development, selection, and evaluation.

The statistical analysis and data processing mentioned above were carried out using Python. Specifically, the fitting and prediction of the MLR model were accomplished using the Scipy version 1.10.0, while the visualization was achieved using the Geopandas version 0.12.2 and related dependencies.

3. Results

During the period of 2001–2019, NEC, NC, and CC were the main regions where wildfires occurred in mainland China, accounting for approximately 28.49%, 19.81%, and 34.55% of the total burned area (BA), respectively. SC, SEC, NWC, and SWC accounted for about 7.16%, 6.35%, 3.23%, and 4.12%, respectively. The variations of the fire season showed certain spatial distribution patterns. Most southern regions (SWC, SC, and CC) had their fire seasons concentrated from January to June (1–6), with a shorter average duration of the fire season (3 months; see Figure 4. In contrast, northern regions (NWC, NC, and NEC) had their fire season concentrated from February to October (2–10), with a longer average duration of the fire season (7.33 months; see Figure 4. SEC is the region with the lowest latitude, and its fire season lasts almost all year round (from January to November; see Figure 4.

To capture the impacts of concurrent and antecedent droughts, we calculated the average drought index (SPEI/sc-PDSI) during the fire season. Additionally, we set a buffer of 2–14 months before the start of the fire season to differentiate between concurrent and antecedent droughts. For each buffer, we calculated the average for 1–12 months. Therefore, there are 156 antecedent drought indicators and 1 concurrent drought indicator and 1 time variable for each region. Finally, we considered these combinations of predictors: concurrent drought only, antecedent drought only, concurrent drought plus time, antecedent

drought plus time, and concurrent and antecedent drought plus time. Overall, we fitted 470 models (1 + 156 + 1 + 156 + 156) for each region and selected the model based on the AIC criterion. The identified key variables can be considered as potential predictors for each region. The concurrent drought is a potential predictor for NEC and SEC (Figure 5a), while the antecedent drought is a potential predictor for all regions except SEC (Figure 5b). In addition, the time variable is a potential predictor for NWC, CC, and NEC (Figure 5c). Figure 2a–c show the coefficients for concurrent drought, antecedent drought, and time, respectively. These coefficients indicate the sensitivity of BA to the predictors. Except for the antecedent drought coefficient for NEC, all drought coefficients are negative. The average coefficient for concurrent drought is −0.65, and the average coefficient for antecedent drought is −2.73 (for all regions, Table 1). The models show that, except for NEC, as the drought indicators decreases (i.e., drier climate conditions), BA increases. The model for NEC shows that if the concurrent drought indicator decreases (i.e., drier climate conditions), BA increases accordingly. However, if the previous winter was drier (antecedent drought indicator for NEC from September to December of the previous year), BA decreases. The time coefficient indicates that from 2001 to 2019, there was a slow declining trend in BA in the NWC and CC regions (Table 1), while the BA in the NEC region showed a slow increasing trend (Figure 5c).
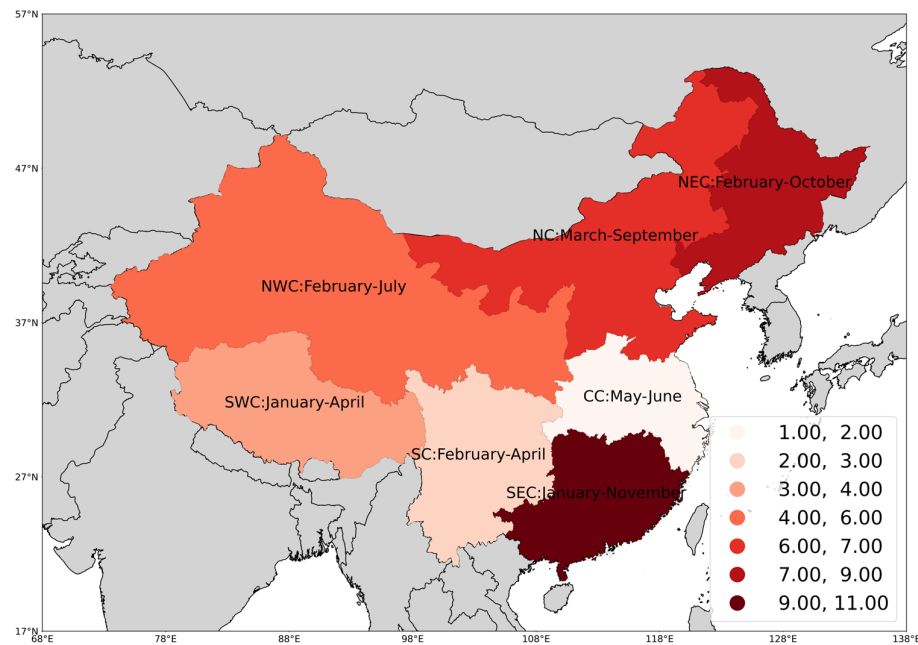
Figure 4. Seasonal Distribution of Regional Fires in China. The figure displays the start and end months of the fire season, with the duration of the fire season represented by the color intensity. The creation of this figure utilized Geopandas version 0.12.2.
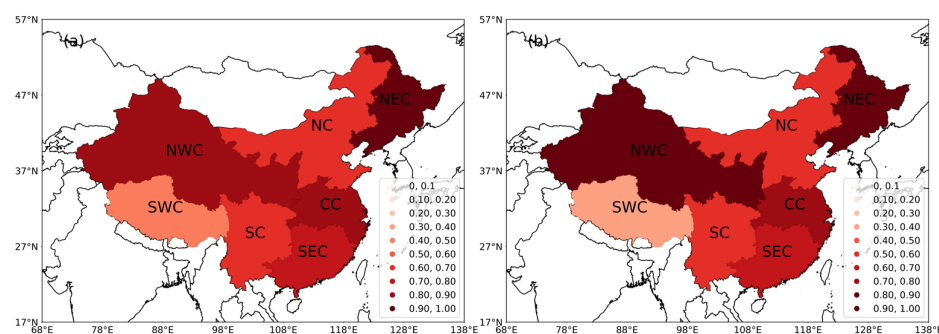
Table 1. Empirical drought-BA model (Equation (1)) for each region. RhoIN, correlation between predicted BA and observed BA (in-sample); RhoOUT, correlation between predicted BA and observed BA (leave-one-out cross-validation).

Region	Model	RhoIN	RhoOUT
NEC	$\log_{10}[\text{BA}(t)] = -1.45 - 0.57 \cdot \text{SPEI}_{9,10,0}(t) + 0.25$ $\cdot \text{SPEI}_{1,2,3}(t) + 0.14 \cdot \text{T}(t) + \varepsilon$	0.92	0.88
NWC	$\log_{10}[\text{BA}(t)] = 1.45 - 0.45 \cdot \text{SPEI}_{2,2,3}(t) - 0.15 \cdot \text{T}(t) + \varepsilon$	0.87	0.80
NC	$\log_{10}[\text{BA}(t)] = -0.63 \cdot \text{SPEI}_{1,3,6}(t) + \varepsilon$	0.63	0.50
SWC	$\log_{10}[\text{BA}(t)] = -0.49 \cdot \text{SPEI}_{1,1,8}(t) + \varepsilon$	0.49	0.31
SC	$\log_{10}[\text{BA}(t)] = -0.65 \cdot \text{SPEI}_{6,2,2}(t) + \varepsilon$	0.65	0.54
CC	$\log_{10}[\text{BA}(t)] = 0.62 - 0.76 \cdot \text{PDSI}_{2,5,2}(t) - 0.06 \cdot \text{T}(t) + \varepsilon$	0.84	0.76
SEC	$\log_{10}[\text{BA}(t)] = -0.74 \cdot \text{SPEI}_{11,11,0}(t) + \varepsilon$	0.74	0.66
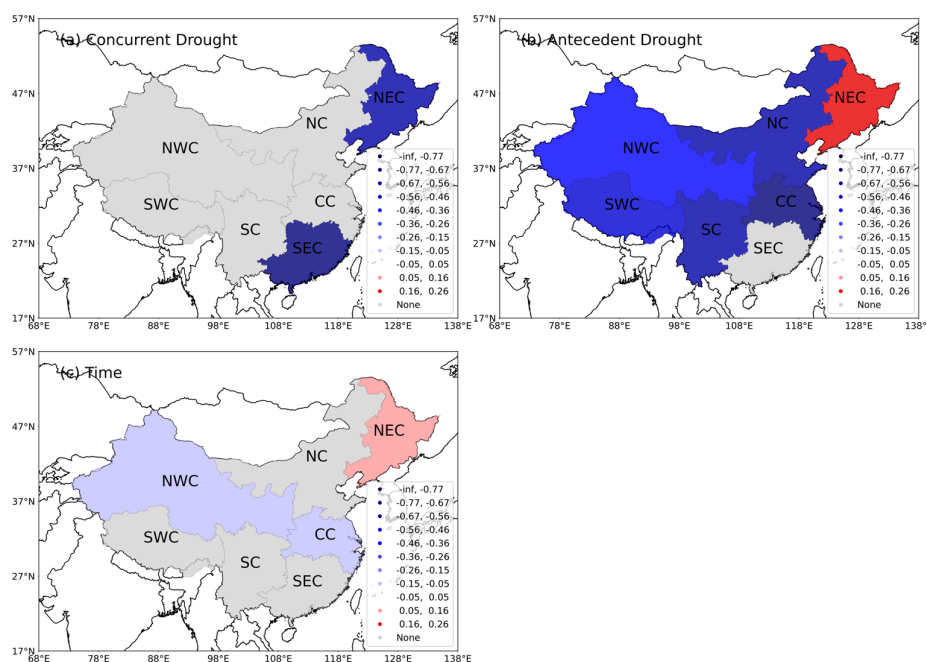
Figure 5. MLR results: (**a**) coefficient for the concurrent drought conditions; (**b**) coefficient for the antecedent drought conditions; (**c**) coefficient weights for the time variable. This figure was created with Geopandas version 0.12.2.

We used parsimonious models, as mentioned before, which are models that explain phenomena or predict results using as few parameters or variables as possible. Figure 6a shows the correlation coefficient (RhoIN) between the in-sample model fit values and the observed values. (The precise definition of each regional model is shown in Table 1.) The average of the correlations for all models is 0.73. Additionally, an important test for these models is to verify their ability to predict out-of-sample data (obtained through leave-one-out cross-validation). Figure 6b shows the correlation coefficient (RhoOUT) between the out-of-sample model fit values and the observed values. The average of the correlations for all models is 0.63. This indicates that the models have relatively good predictive power.

Figure 6. MLR results: (**a**) correlation between predicted BA and observed BA (in-sample); (**b**) correlation between predicted BA and observed BA (leave-one-out cross-validation). This figure was created with Geopandas version 0.12.2.

4. Discussion

Climate plays a significant role in influencing the likelihood, intensity, and frequency of wildfires. Changes in climate patterns, such as temperature and precipitation, can create conditions that increase the risk of wildfires [40]. In addition, human activities such as land-use change and fire-suppression policies can exacerbate the effects of climate change on wildfire [41,42]. Due to China's enormous population, diverse climatic conditions, and vegetation types, there are considerable regional variations in the spatial and temporal

distribution characteristics of wildfires. Nevertheless, we found that the fire season shows a spatial variation pattern that increases with latitude. In addition, NEC, NC, and CC were the main regions where wildfires occurred in mainland China. The spatial distribution of burned area (BA) is consistent with the results of many independent studies [24,43,44] but not consistent with the spatial distribution of fire frequency [45]. These results indicate the BA in the north of China may be larger than that in the south, but the frequency is lower.

In this study, we present a series of multiple linear regression (MLR) models linking burned area (BA) during mainland China's fire season from 2001 to 2019 and across seven regions to concurrent drought, antecedent drought, and time trend. Specifically, we investigated the dependency of wildfires during the fire season on concurrent drought conditions, which affect the dryness of fuel through climatic factors, as well as antecedent drought conditions, which impact the fuel load and the fine fuel structure through climate factors. It is worth noting that most regions included antecedent drought in their models, while only two regions included concurrent drought. This result differs significantly from that of the Mediterranean region [13,46]. Possible reasons for this discrepancy include the following: (1) The measurement of concurrent drought was solely based on the average values during the fire season, while the time window for antecedent drought was more extensive, and (2) concurrent drought may be highly correlated with early-stage drought and was thus excluded during model selection. (Studies have shown a clear drought trend throughout China [47].) In the case of China, Zhao [16] conducted a comparison of the fitting capabilities of different climate factors using a univariate linear regression approach. The study categorized the observed series into three groups: above normal, normal, and below normal. The assessment of the model's fitting capability was based on the count of observations and fitted values that fell into the above-normal category simultaneously. In our research, we rigorously evaluated the model's fitting capability and achieved higher rates of fit in most regions compared to the predictive fitting rates reported in Zhao's study.

The specific reasons warrant further investigation. The study is a necessary step in addressing the question of whether climate change will increase wildfire activity in China. The impact of climate change on wildfire activity is complex, as an increase in fire weather can be exacerbated or offset by changes in vegetation productivity [9].

The statistical analysis reported here indicates that concurrent drought conditions play a dominant role in the occurrence of fires in the NEC ($\beta_1 > \beta_2$) and SEC regions. The NEC region experiences high summer temperatures (averaging approximately 30 °C) and cold, dry winters (averaging approximately -30 °C). The majority of the annual rainfall occurs during the summer (around 500 mm) [48]. Temperatures gradually increase beginning in March, leading to melting snow and ice and a moistening of the land. Starting in October each year, temperatures significantly drop [49]. The main forest type is deciduous coniferous forest, which is difficult to dry and therefore has a relatively long fire season. However, the wood contains a large amount of resin, making it prone to large fires. A particularly interesting aspect is that the wetter climate conditions last year also led to an increase in BA in the NEC region. This may be because the previous wetter climate helped plant growth and ensured the continuity of fuels. The SEC region experiences consistently high temperatures throughout the year [50], leading to a prolonged fire season that spans from January to November. However, the SEC region has an annual average rainfall of up to 1780 mm [51], which results in not much burned area (BA). There is a moist humus layer under the forest, and the continuous high temperature in the fire season will make it dry, causing frequent fire. However, rainfall and a humid climate generally prevent large-scale fires in this area [45].

Antecedent drought is the key predictor in most regions, which may be because the fuel load and factors related to ignition are controlled by previous climatic conditions. For instance, drying of fine fuels during the early months of the fire season may encourage wildfire activity [38,52]. Fire occurrence is determined by a delicate balance between vegetation productivity (fuel production) and the frequency of dry conditions (fuel moisture) [9]. Most eastern regions (NC, CC, and SC) are more sensitive to antecedent drought than

western regions (SWC and NWC). This is maybe due to the large terrain, low population density, limited vegetation coverage, and small BA in the western region (SWC and NWC). Its fuel load and continuity are considerably weaker when confronted with a variety of ecological issues including desertification, local forest destruction, grassland degradation, etc. [53–57].

In NWC and CC regions, the results of the model show that BA decreases slowly with time. This may be the result of a combination of vigilance and a set of preventive measures coordinated by local authorities, firefighters, and forest managers. The NEC region shows a trend of slow growth over time, which may be the impact of climate warming.

5. Conclusions

In general, SPEI and sc-PDSI demonstrate good applicability in the seven regions of China, although there are variations in the time window across different regions. The linear regression models we developed demonstrate relatively high ability in both the within-sample and out-sample. These relatively simple regression models link drought index with fire activity, which can be used to estimate the response of fires in the Chinese mainland to different climate-change scenarios, assuming that the climate–vegetation–human–fire interaction and its feedback do not change significantly. However, the complex relationship between fire, climate change, human activities, and vegetation distribution may limit the applicability of these findings under very different conditions from the current situation. Future research lines should take into account a wide range of vegetation, human, and meteorological factors. The models showed good predictive power, indicating their potential usefulness in predicting future wildfire occurrences. Overall, these findings provide valuable insights into the spatial distribution and potential predictors of wildfires in mainland China, which can inform wildfire management and prevention strategies.

Author Contributions: Conceptualization, S.Y., A.Z. and F.G.; methodology, S.Y. and A.Z.; software, S.Y.; validation, Z.Z. and H.Z.; formal analysis, S.Y. and A.Z.; investigation, S.Y., A.Z. and F.G.; resources, S.Y., A.Z. and F.G.; data curation, Z.Z. and H.Z.; writing—original draft preparation, S.Y. and A.Z.; writing—review and editing, S.Y., A.Z., M.T., G.W. and F.G.; visualization, S.Y. and A.Z.; supervision, M.T., G.W. and F.G.; project administration, F.G.; funding acquisition, F.G. All authors have read and agreed to the published version of the manuscript.

Institutional Review Board Statement: Not applicable.

Informed Consent Statement: Not applicable.

Data Availability Statement: The data presented in this study are available on request from the corresponding author.

Conflicts of Interest: The authors declare no conflict of interest.

References

1. Mansoor, S.; Farooq, I.; Kachroo, M.M.; Mahmoud, A.E.D.; Fawzy, M.; Popescu, S.M.; Alyemeni, M.N.; Sonne, C.; Rinklebe, J.; Ahmad, P. Elevation in wildfire frequencies with respect to the climate change. *Environ. Manag.* **2022**, *301*, 113769. [CrossRef]
2. Mays, C.; Mcloughlin, S. End-permain burnout: The role of permain-triassic wildfires in extinction, carbon cycling, and environmental change in Eastern Gondwana. *Palaios* **2022**, *37*, 292–317. [CrossRef]
3. Westerling, A.L. Increasing western US forest wildfire activity: Sensitivity to changes in the timing of spring. *Philos. Trans. R. Soc. B Biol. Sci.* **2016**, *371*, 20150178. [CrossRef]
4. Field, R.D.; Werf, G.R.; Shen, S.S.P. Human amplification of drought-induced biomass burning in Indonesia since 1960. *Nat. Geosci.* **2009**, *2*, 185–188. [CrossRef]
5. Brown, T.; Leach, S.; Wachter, B.; Gardunio, B. The Extreme 2018 Northern California Fire Season. *Bull. Am. Meteorol. Soc.* **2020**, *101*, S1–S4. [CrossRef]
6. Boer, M.M.; Nolan, R.H.; Resco De Dios, V.; Clarke, H.; Price, O.F.; Bradstock, R.A. Changing Weather Extremes Call for Early Warning of Potential for Catastrophic Fire. *Earths Future* **2017**, *5*, 1196–1202.
7. Pausas, J.G.; Keeley, J.E. A Burning Story: The Role of Fire in the History of Life. *BioScience* **2009**, *59*, 593–601. [CrossRef]

8. Pausas, J.G.; Ribeiro, E. The global fire-productivity relationship. *Glob. Ecol. Biogeogr.* **2013**, *22*, 728–736. [CrossRef]
9. Jones, M.W.; Abatzoglou, J.T.; Veraverbeke, S.; Andela, N.; Lasslop, G.; Forke, M.; Smith, A.J.P.; Burton, C.; Betts, R.A.; Werf, G.R.; et al. Global and Regional Trends and Drivers of Fire Under Climate Change. *Rev. Geophys.* **2022**, *60*, 1–76. [CrossRef]
10. Archibald, S.; Roy, D.P.; Wilgen, B.W.; Scholes, R.J. What limits fire? An examination of drivers of burnt area in Southern Africa. *Glob. Chang. Biol.* **2009**, *15*, 613–630. [CrossRef]
11. Kelley, D.I.; Bistinas, I.; Whitley, R.; Burton, C.; Marthews, T.R.; Dong, N. How contemporary bioclimatic and human controls change global fire regimes. *Nat. Clim. Chang.* **2019**, *9*, 690–696. [CrossRef]
12. Parisien, M.A.; Moritz, M.A. Environmental controls on the distribution of wildfire at multiple spatial scales. *Ecol. Monogr.* **2009**, *79*, 127–154. [CrossRef]
13. Turco, M.; von Hardenberg, J.; AghaKouchak, A.; Trigo, R.M. On the key role of droughts in the dynamics of summer fires in Mediterranean Europe. *Sci. Rep.* **2017**, *7*, 81. [CrossRef] [PubMed]
14. Ruffault, J.; Moron, V.; Trigo, R.M.; Curt, T. Objective identification of multiple large fire climatologies: An application to a Mediterranean ecosystem. *Environ. Res. Lett.* **2016**, *11*, 075006. [CrossRef]
15. Swetnam, T.W.; Betancourt, J.L. Mesoscale Disturbance and Ecological Response to Decadal Climatic Variability in the American Southwest. *J. Clim.* **1998**, *11*, 3128–3147. [CrossRef]
16. Zhao, F.; Liu, Y. Important Meteorological Predictors for Long-Range Wildfires in China. *For. Ecol. Manag.* **2021**, *499*, 119638. [CrossRef]
17. Wells, N.; Goddard, S.; Hayes, M.J. Self-Calibrating Palmer Drought Severity Index. *J. Clim.* **2004**, *17*, 2335–2351. [CrossRef]
18. Palmer, W.C. *Meteorological Drought*; Office of Climatology Research Paper 45; Weather Bureau: Washington, DC, USA, 1965.
19. Vicente-Serrano, S.M.; Beguería, S.; López-Moreno, J.I.A. Multiscalar Drought Index Sensitive to Global Warming: The Standardized Precipitation Evapotranspiration Index. *J. Clim.* **2010**, *23*, 1696–1718. [CrossRef]
20. Yu, L.; Zhong, S.; Sun, B. The Climatology and Trend of Surface Wind Speed over Antarctica and the Southern Ocean and the Implication to Wind Energy Application. *Atmosphere* **2020**, *11*, 108–127. [CrossRef]
21. You, Q.; Wu, T.; Shen, L.; Pepin, N.; Zhang, L.; Jiang, Z.; Wu, Z.; Kang, S.; AghaKouchak, A. Review of Snow Cover Variation over the Tibetan Plateau and Its Influence on the Broad Climate System. *Earth-Sci. Rev.* **2020**, *201*, 103043. [CrossRef]
22. Fang, Z.; Liu, Z.; He, C.; Tu, M.; Zhao, R.; Lu, W. Will climate change make Chinese people more comfortable? A scenario analysis based on the weather preference index. *Environ. Res. Lett.* **2020**, *15*, 084028. [CrossRef]
23. Chang, Y.; Zhu, Z.; Bu, R.; Li, Y.; Hu, Y. Environmental controls on the characteristics of mean number of forest fires and mean forest area burned (1987–2007) in China. *For. Ecol. Manag.* **2015**, *356*, 13–21. [CrossRef]
24. Zhao, F.; Liu, Y. Atmospheric Circulation Patterns Associated with Wildfires in the Monsoon Regions of China. *Geophys. Res. Lett.* **2019**, *46*, 4873–4882. [CrossRef]
25. Morisette, J.T.; Giglio, L.; Csiszar, I.; Justice, C.O. Validation of the MODIS active fire product over Southern Africa with ASTER data. *Int. J. Remote Sens.* **2005**, *26*, 4239–4264. [CrossRef]
26. Morisette, J.T.; Giglio, L.; Csiszar, I.; Setzer, A.; Schroeder, W.; Morton, D.; Justice, C.O. Validation of MODIS Active Fire Detection Products Derived from Two Algorithms. *Earth Interact.* **2005**, *9*, 1–25. [CrossRef]
27. Csiszar, I.; Morisette, J.; Giglio, L. Validation of active fire detection from moderate-resolution satellite sensors: The MODIS example in northern Eurasia. *IEEE Trans. Geosci. Remote Sens.* **2006**, *44*, 1757–1764. [CrossRef]
28. Schroeder, W.; Prins, E.; Giglio, L.; Csiszar, I.; Schmidt, C.; Morisette, J.; Morton, D. Validation of GOES and MODIS active fire detection products using ASTER and ETM+ data. *Remote Sens. Environ.* **2008**, *112*, 2711–2726. [CrossRef]
29. Climatic Research Unit. CRU TS4.05: Climatic Research Unit (CRU) Time-Series (TS) Version 4.05 of High-Resolution Gridded Data of Month-by-Month Variation in Climate (January 1901–December 2020). NERC EDS Centre for Environmental Data Analysis. 2021. Available online: https://catalogue.ceda.ac.uk/uuid/c26a65020a5e4b80b20018f148556681 (accessed on 8 February 2023).
30. Harris, I.; Osborn, T.J.; Jones, P.; Lister, D. Version 4 of the CRU TS monthly high-resolution gridded multivariate climate dataset. *Sci. Data* **2020**, *7*, 109. [CrossRef]
31. Barichivich, J.; Osborn, T.; Harris, I.; Schrier, G.; Jones, P. Drought: Monitoring global drought using the self-calibrating Palmer Drought Severity Index. *Bull. Am. Meteorol. Soc.* **2019**, *100*, S39–S40.
32. Jain, P.; Wang, X.; Flannigan, M.D. Trend analysis of fire season length and extreme fire weather in North America between 1979 and 2015. *Int. J. Wildland Fire* **2017**, *26*, 1009. [CrossRef]
33. Bedia, J.; Herrera, S.; Gutiérrez, J.M.; Benali, A.; Brands, S.; Mota, B.; Moreno, J.M. Global patterns in the sensitivity of burned area to fire-weather: Implications for climate change. *Agric. For. Meteorol.* **2015**, *214–215*, 369–379. [CrossRef]
34. Andela, N.D.; Morton, C.; Giglio, L.; Chen, Y.; Werf, G.R.; Kasibhatla, P.S.; DeFries, R.S.; Collatz, G.J.; Hantson, S.; Kloster, S.; et al. A human-driven decline in global burned area. *Science* **2017**, *356*, 1356–1362. [CrossRef] [PubMed]
35. Knorr, W.; Kaminski, T.; Arneth, A.; Weber, U. Impact of human population density on fire frequency at the global scale. *Biogeosciences* **2014**, *11*, 1085–1102. [CrossRef]
36. Littell, J.S.; Peterson, D.L.; Riley, K.L.; Liu, Y.; Luce, C.H. A review of the relationships between drought and forest fire in the United States. *Glob. Chang. Biol.* **2016**, *22*, 2353–2369. [CrossRef]
37. Abatzoglou, J.T.; Williams, A.P.; Boschetti, L.; Zubkova, M.; Kolden, C.A. Global patterns of interannual climate–fire relationships. *Glob. Chang. Biol.* **2018**, *24*, 5164–5175. [CrossRef]

38. Archibald, S.; Lehmann, C.E.R.; Gómez-Dans, J.L.; Bradstock, R.A. Defining pyromes and global syndromes of fire regimes. *Proc. Natl. Acad. Sci. USA* **2013**, *110*, 6442–6447. [CrossRef]

39. Akaike, H. A new look at the statistical model identification. *IEEE Trans. Autom. Control* **1974**, *19*, 716–723. [CrossRef]

40. Schoennagel, T.; Balch, J.K.; Brenkert-Smith, H.; Dennison, P.E.; Harvey, B.J.; Krawchuk, M.A.; Mietkiewicz, N.; Morgan, P.; Moritz, M.A.; Rasker, R.; et al. Adapt to more wildfire in western North American forests as climate changes. *Proc. Natl. Acad. Sci. USA* **2017**, *114*, 4582–4590. [CrossRef]

41. Abatzoglou, J.T.; Williams, A.P. Impact of anthropogenic climate change on wildfire across western US forests. *Proc. Natl. Acad. Sci. USA* **2016**, *113*, 11770–11775. [CrossRef]

42. Flannigan, M.D.; Krawchuk, M.A.; de Groot, W.J.; Wotton, B.M.; Gowman, L.M. Implications of changing climate for global wildland fire. *Int. J. Wildland Fire* **2009**, *18*, 483. [CrossRef]

43. Ying, L.; Han, J.; Du, Y.; Shen, Z. Forest fire characteristics in China: Spatial patterns and determinants with thresholds. *For. Ecol. Manag.* **2018**, *424*, 345–354. [CrossRef]

44. Dios, V.R.; de Yao, Y.; Camprubí, À.C.; Boer, M.M. Fire activity as measured by burned area reveals weak effects of ENSO in China. *Nat. Commun.* **2022**, *13*, 4316. [CrossRef]

45. Fang, K.; Yao, Q.; Guo, Z.; Zheng, B.; Du, J.; Qi, F.; Yan, P.; Li, J.; Ou, T.; Liu, J.; et al. ENSO modulates wildfire activity in China. *Nat. Commun.* **2021**, *12*, 1764. [CrossRef]

46. Marco, T.; José, R.-C.J.; Joaquín, B.; Sonia, J.; Pedro, M.J.; Carmen, L.M.; Antonello, P. Exacerbated fires in Mediterranean Europe due to anthropogenic warming projected with non-stationary climate-fire models. *Nat. Commun.* **2018**, *9*, 3821.

47. Shao, D.; Chen, S.; Tan, X.; Gu, W. Drought characteristics over China during 1980–2015. *Int. J. Climatol.* **2018**, *38*, 3532–3545. [CrossRef]

48. Tian, X.; McRae, D.J.; Jin, J.; Shu, L.; Zhao, F.; Wang, M. Wildfires and the Canadian Forest Fire Weather Index system for the Daxing'anling region of China. *Int. J. Wildland Fire* **2011**, *20*, 963–973. [CrossRef]

49. Zhao, F.; Liu, Y.; Shu, L. Change in the fire season pattern from bimodal to unimodal under climate change: The case of Daxing'anling in Northeast China. *Agric. For. Meteorol.* **2020**, *291*, 108075. [CrossRef]

50. Zhu, K.; Qiu, X.; Luo, Y.; Dai, M.; Lu, X.; Zang, C.; Zhang, W.; Gan, X.; Zhula, W. Spatial and temporal dynamics of water resources in typical ecosystems of the Dongjiang River Basin, China. *J. Hydrol.* **2022**, *614*, 128617. [CrossRef]

51. Yuan, Z.; Liang, C.; Li, D. Urban stormwater management based on an analysis of climate change: A case study of the Hebei and Guangdong provinces. *Landsc. Urban Plan.* **2018**, *177*, 217–226. [CrossRef]

52. Knorr, W.; Arneth, A.; Jiang, L. Demographic controls of future global fire risk. *Nat. Clim. Chang.* **2016**, *6*, 781–785. [CrossRef]

53. He, J.; Pan, Z.; Liu, D.; Guo, X. Exploring the regional differences of ecosystem health and its driving factors in China. *Sci. Total Environ.* **2019**, *673*, 553–564. [CrossRef] [PubMed]

54. Aishan, T.; Halik, Ü.; Kurban, A.; Cyffka, B.; Kuba, M.; Betz, F.; Keyimu, M. Eco-morphological response of floodplain forests (*Populus euphratica* Oliv.) to water diversion in the lower Tarim River, northwest China. *Environ. Earth Sci.* **2014**, *73*, 533–545. [CrossRef]

55. Zhang, G.Q.; Xie, H.J.; Yao, T.D.; Kang, S.C. Water balance estimates of ten greatest lakes in China using ICESat and Landsat data. *Chin. Sci. Bull.* **2013**, *58*, 3815–3829. [CrossRef]

56. Zhou, W.; Gang, C.; Zhou, l.; Chen, Y.; Li, J.; Ju, W.; Odeh, I. Dynamic of grassland vegetation degradation and its quantitative assessment in the northwest China. *Acta Oecol.* **2014**, *55*, 86–96. [CrossRef]

57. Zhang, Z.; Xia, f.; Yang, D.; Huo, J.; Chen, H. Spatiotemporal characteristics in ecosystem service value and its interaction with human activities in Xinjiang, China. *Ecol. Indic.* **2020**, *110*, 105826. [CrossRef]